Progress In Electromagnetics Research C, Vol. 90, 237–252, 2019

Path Loss Measurement and Prediction in Outdoor Fruit Orchard for Wireless Sensor Network at 2.4 GHz Band

Tossaporn Srisooksai[1, *], Kamol Kaemarungsi[2], Junichi Takada[3], and Kentaro Saito[3]

Abstract—This work describes the path loss of radio propagation for wireless sensor network in the outdoor fruit orchard which is one of the common agriculture environments. The measurement was conducted in the jackfruit orchard in the 2.45 GHz band. Unlike other studies conducted in the fruit orchard environments, the variation of path loss over the relative angles between the plant rows and the line-of-sight direction from the transmitter to the receiver is identified. The equivalent vegetation obstruction model is proposed as the function of the equivalent number of trees along the line-of-sight to better represent the angular path loss variation. This leads to the proposal of the path loss prediction approach at any point in the fruit orchard by using a few measurement efforts. This work also introduces the Monte Carlo simulation using the numerical electromagnetic scattering computation called hybrid T-matrix method to evaluate the relative angular vegetation loss of a single tree that is used as the input to determine the equivalent number of trees. The evaluation results suggest that it can further reduce the measurement workload required for the proposed path loss prediction approach.

1. INTRODUCTION

Recently, the wireless sensor network (WSN) has been applied to gather the variability of environmental parameters in the agriculture fields, thus precision management can be applied to improve the yield [1]. For the gathering application, several sensor nodes are distributed around a wide geographical area in which the reliability of wireless communication in terms of network coverage is essential [2]. [2] showed that information of radio propagation channel parameters such as path loss helps achieve this requirement.

Considerable works [3–9] have investigated and empirically modeled the path loss in the forest. These empirical models might be applicable to the agricultural fruit orchards because they are also dominated by trees with a single trunk. However, the special characteristics of the fruit orchards that differ from the forest environments might limit such the model applicability. These characteristics include the periodic distribution of the trees in the orchard with the grid manner, as well as the leaf density, canopy size, and trunk size which are similar over the trees since they have the same age of growth. On the other hand, in the forest environments, the tree distribution in the space, leaf density, canopy size, and trunk size are random. On the basis of these randomnesses, the same empirical model may be used to predict the path loss in any angular direction in the forest, but the same angular path loss model may not be applicable to the grid planting pattern of the fruit orchards.

In the authors' previous work [10], the path loss in the agricultural sugarcane field, where the crops are planted in the ridge pattern, was investigated. The high variation of path loss was observed over the angular directions. The definition of angular direction is the relative angle between the plant

Received 19 November 2018, Accepted 13 January 2019, Scheduled 5 March 2019

* Corresponding author: Tossaporn Srisooksai (srisooksai@ap.ide.titech.ac.jp).

[1] Graduate School of Science and Engineering, Tokyo Institute of Technology, Japan. [2] National Electronics and Computer Technology Center (NECTEC), Pathumthani, Thailand. [3] School of Environment and Society, Tokyo Institute of Technology, Japan.

rows and the line-of-sight (LOS) direction from the transmitting antenna (Tx) to the receiving antenna (Rx). The results revealed that the number of ridges existing along the LOS of the Tx and Rx is the dominant cause of the angular variation. This number of ridges represents the magnitude of vegetation obstruction. Therefore, the vegetation obstruction (VO) model was proposed to better represent such a variation.

Although the path loss results in various types of outdoor fruit orchards for various frequencies and different antenna heights were investigated through the measurements in the existing works [2, 11–13], the effect of the angular direction and the loss due to vegetation obstruction existing along the LOS of the Tx and Rx on the path loss in the fruit orchards have not been studied. In addition, the VO model proposed for the sugarcane field, which is classified as the tall food grass environment, is not applicable to the fruit orchard due to the different characteristics of the species, as well as the planting patterns [10].

Compared with existing studies, the contributions of this paper are summarized as follows. First, the influence of the angular direction, α, and the number of trees existing along the LOS, n, on the path loss is clarified through measurements in a jackfruit orchard. Observing that n can be counted as 1 only when the LOS of the Tx and Rx is passing through the center of a tree, the concept of the equivalent number of trees along the LOS, n_{t}, is introduced to represent n in any angular direction. Second, the results reveal that n_{t} is a significant cause of the angular path loss variation. The equivalent vegetation obstruction (EVO) model is proposed as the semi-empirical function of n_{t} to better represent such an angular variation. This leads to the procedure of the path loss prediction approach at any point in the jackfruit orchard by making a few measurement efforts. Although further experimental validation is needed, the same procedure is expected to be applicable to other fruit orchards under the conditions described in this work. Third, this work introduces the Monte Carlo simulation using the numerical electromagnetic scattering computation called hybrid T-matrix method [14, 15] to evaluate the relative angular vegetation loss of a single tree that is used as the input to determine n_{t}. The evaluation results suggest that it can further reduce the measurement workload required for the proposed path loss prediction procedure. In this work, the results in the 2.4 GHz band are reported because it suffers from a relatively higher theoretical propagation loss, and thus it has more difficulty in managing the radio coverage than in sub 1 GHz band applied in the WSN such as 868 and 920 MHz, while it is able to provide higher data transmission [16].

The rest of this paper is organized as follows. The related works of existing modeling approaches in vegetation environment, as well as the electromagnetic scattering computation approach for the vegetation medium, are briefly described in Section 2. The measurement campaign in the jackfruit orchard is explained in Section 3. The data processing for estimating the path loss is briefly described in Section 4. The differences between the modeling approaches used in this work and the existing work are highlighted in Section 5 including the detail of determining n_{t} using the relative angular vegetation loss of a single tree. In Section 6, the results of the relative angular vegetation loss of a single tree obtained from the measurement and the Monte Carlo simulation using hybrid T-matrix are compared and presented, and the measurement results of path loss are presented using the proposed model. The prediction procedure of the path loss at any point in the fruit orchard is proposed and discussed in Section 7. Finally, the conclusions are given in Section 8.

2. RELATED WORKS

2.1. Existing Path Loss Modeling

This work mainly refers to the existing modeling approaches and the mathematical notations that are described and defined in [10], respectively. The brief details are given here for the completeness. In vegetation environment, the path loss is typically modeled [7, 9, 10, 13] as

$$\tilde{L}(d_{\mathrm{t}}) = F(d_{\mathrm{t}}) + \tilde{X}(d),\ \mathrm{dB} \tag{1}$$

where d_{t} is the distance between the Tx and Rx, and d is the vegetation depth. $\tilde{X}$ is the vegetation attenuation model of the excess loss, X, which is generally defined as the path loss value, L, that exceeds the free space loss, F. L and X are obtained from the measurement, whereas $\tilde{L}$ and $\tilde{X}$ are used to represent the models of L and X, respectively.

2.1.1. Empirical Model

The vegetation attenuation models, $\tilde{X}$, which are classified into analytical and empirical models, are comprehensively presented in [17]. Only a brief summary of empirical models is given here. The broadly recognized empirical generic models for X are the modified exponential decay (MED) model and modified gradient model. The existing models consider only the distance parameter, whereas the VO model, which considers the number of ridges (obstructions) along the LOS of the Tx and Rx, was proposed in [10] for the tall food grass field.

- **Modified exponential decay model**: MED model is sometimes called as COST 235 model [18]. It is expressed as

$$\tilde{X}_{\text{med}}(d) = U f^V d^W, \text{ dB} \tag{2}$$

where f is the frequency, and U, V, and W are the fitting parameters.

- **Modified gradient model**: It was intentionally proposed to represent two gradients of the attenuation rate observed through the measurements in which the initial gradient of the attenuation increases rapidly over shorter d, while the final gradient of the attenuation is considerably slower at large d [19]. There are two models in this group: maximum attenuation (MA) model [9] and non-zero gradient (NZG) model [19] described as (3) and (4), respectively:

$$\tilde{X}_{\text{ma}}(d) = A_{\text{m}} \left\{ 1 - \exp\left(-\frac{R_0}{A_{\text{m}}} d \right) \right\}, \text{ dB} \tag{3}$$

$$\tilde{X}_{\text{nzg}}(d) = R_\infty d + M \left\{ 1 - \exp\left(-\frac{R_0 - R_\infty}{M} d \right) \right\}. \text{ dB} \tag{4}$$

In these models, R_0 (dB/m) and R_∞ (dB/m) represent the initial and final gradients of the attenuation rate of X, respectively, whereas A_{m} (dB) in Eq. (3) and M (dB) in Eq. (4) represent the maximum and offset of X, respectively.

- **Vegetation obstruction model**: In [10], the number of ridges existing along the LOS of the Tx and Rx, n_{r}, was found to be the reason behind the angular variation in the sugarcane field. Therefore, the VO model is proposed to represent such variation as

$$\tilde{X}_{\text{vo}}(n_{\text{r}}) = A_{\text{evo}} \left\{ 1 - \exp\left(-\frac{R_{\text{vo}}}{A_{\text{evo}}} n_{\text{r}} \right) \right\}, \text{ dB} \tag{5}$$

where R_{vo} and A_{evo} are the initial gradient of the attenuation rate of X over n_{r} and the maximum of X, respectively. In this model, the main assumption is that the vegetation length of each ridge in each angular directions is not significantly different [10]. In other words, n_{r} can be counted as 1 regardless of the LOS along the Tx and Rx passing through a ridge in any angle because the crops are planted and distributed closely in a narrow ridge pattern.

2.2. Hybrid *T*-Matrix Method

The alternative way of predicting the radio propagation is to solve Maxwell's equations in electromagnetic theory. However, due to the complex geometry of the vegetation obstacles in the agriculture field, the exact solution to Maxwell's equations is impractical. Solving Maxwell's equations by the numerical approaches, e.g., finite-difference time-domain (FDTD) [20] and the method of moments (MOM) [21], is also computationally intensive due to the complex geometry and large electrical size of the agriculture crop. In [22, 23], transport theory was applied to obtain the analytical solution for the electromagnetic wave propagation in the forest environment. Such an analytical prediction approach is called radiative energy transfer (RET). However, radio propagation prediction by RET-based approach requires the input parameters from the complicated measurements such as the ratio of the forward scattered power to the total scattered power and the ratio of the scattering cross-section to the total cross-section [22]. Recently, the hybrid T-matrix approach [14, 15] has been developed to determine the electromagnetic scattering from the vegetation structure. Compared with the ordinary numerical approach, larger electrical size can be solved.

It is known that the relationship between the spherical wave coefficients of the incident and scattered waves can be linearly represented by the T-matrix [24]. In [14, 15], the T-matrix of each tree element, such as leaf, branch, and trunk, was determined by the hybrid approach. First, the scattered fields of a single scatterer induced by the multiple incident wave directions are determined using the conventional electromagnetic solvers. In [14, 15], the FEKO software [25], which relies on a MOM solver, was used. Second, the spherical wave coefficients of such a single scatterer are determined using point matching approach [26] in which the coefficients are computed to match the obtained scattered fields at several matching points. Using the known spherical wave coefficients of the incident wave, the T-matrix of a single scatterer can be finally determined. The authors in [14, 15] showed that the total electromagnetic scattered field in the far-field region of the vegetation structure such as tree can be approximated by the superposition of the scattered field of the first-order scattering of each individual tree element determined by using its T-matrix.

3. MEASUREMENT CAMPAIGN

The measurement of the path loss in the jackfruit orchard was conducted in the rural area of Chonburi Province located in the east of Thailand during October 22–27, 2017. The measurement was conducted by using a channel sounder that was specifically designed and developed in [27] for the outdoor agriculture environment. Important parameters of the channel sounder used in the measurement are summarized in Table 1.

Table 1. Channel sounding parameters.

Parameters	Value
Center frequency	2.45 GHz
Number of frequency tones	134
Total bandwidth	45.6 MHz
Frequency tone spacing	343 kHz
Symbol duration	2.9 µs
Delay resolution	21.9 ns
Total measurement time	0.5 s
Antenna for both Tx and Rx.	Directional outdoor WiFi antenna Vertical polarization Vertical beamwidth: 30° Horizontal beamwidth: 30° Gain: 14 dBi, Height: 1.7 m

As in [10], the Tx antenna was fixed at a certain point while the Rx antenna was moved to the specific points and angular directions in the field manually. It takes 0.5 s for one snapshot of the measurement, and the time-invariant condition is assumed due to lack of dynamic movement during the period. A preliminary measurement was also conducted to ensure that there was no radio signal interference from other radio transmission systems.

The area of the jackfruit orchard is $48 \times 24\,\mathrm{m}^2$. The jackfruit tree with a few numbers of jackfruit is shown in Fig. 1(a). The range of tree heights is 5–6 m, and the canopies occupies from 1.3 m above the ground to the top of the tree and spanned in the range of 4 m horizontally. The average trunk diameter at the level of antenna height is 0.1 m. The antenna height was set at 1.7 m which is the same as the height used in the real implementation of WSN in agriculture field [28]. The effect of α on the path loss was investigated. As shown in Fig. 1(b), the case in which the LOS direction is between two rows of the jackfruit trees is defined as $\alpha = 0°$. Even in this angle, a part of the canopy obstructed the LOS. In each α direction, the Tx is placed at the front boundary of the orchard, and the Rx is moved with the steps of 4 to 6 m depending on the obstruction of the trees. The Tx and Rx antennas were oriented

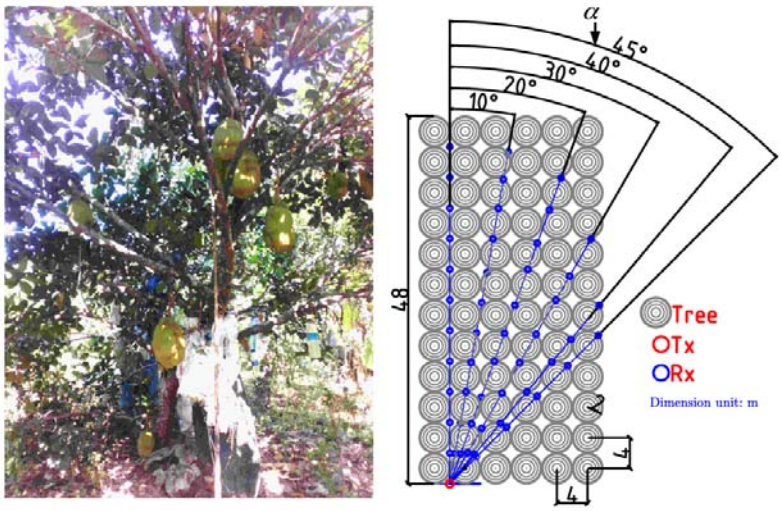

Figure 1. (a) Jackfruit tree. (b) Measurement in the jackfruit orchard from $\alpha = 0°$ to $45°$.

for a maximum response. The same process is repeated for the other angles. In addition, the results of the measurement points, which are angularly located around the closest tree from the Tx shown in Fig. 1(b), will be later used for the analysis of the relative vegetation loss of a single tree.

4. PATH LOSS ESTIMATION

This work follows the data processing described in [10, Subsection 4.1] to estimate the path loss value, L, of each measurement point which is represented by d and α defined in Fig. 1(b). This data processing is briefly explained here for completeness. The output of the channel sounder is the 45.6 MHz bandwidth channel transfer function, $H[t,k]$, of each measurement point, where $k = 1, 2, \ldots, K$ denotes the frequency index; K is the number of frequency tones shown in Table 1; $t = 1, 2, \ldots, T$ represents the snapshot index; and a snapshot duration equals a symbol duration, as shown in Table 1. Then the Tx antenna gain, g_{Tx}, and the Rx antenna gain, g_{Rx}, are eliminated as

$$\hat{H}[t,k,d,\alpha] = \frac{H[t,k,d,\alpha]}{\sqrt{g_{\mathrm{Tx}} g_{\mathrm{Rx}}}}. \tag{6}$$

The average path gain value, G, of each measurement point can be obtained by averaging the power of $\hat{H}[t,k]$ over k and t as

$$G[d,\alpha] = \frac{1}{KT} \sum_{t=1}^{T} \sum_{k=1}^{K} |\hat{H}[t,k,d,\alpha]|^2. \tag{7}$$

This average is applied in order to remove the small-scale fading due to the superposition of the multipath components. Then, the path loss value L of each measurement point, which is the inverse path gain ratio, is obtained. Because the noise floor of the receiver after removing the antenna gain is -113 dB, only the measurement points where L is smaller than 108 dB (another 5 dB is the safety margin) are considered. The excess loss, X, of each measurement point is then obtained by removing F from L as

$$X[d,\alpha] = L[d,\alpha] - F(d). \text{ dB} \tag{8}$$

5. PROPOSED APPROACHES

This section describes the differences between the existing modeling approaches described in Section 2 and the alternative approaches used in this work.

5.1. Proposed Excess Loss Model

In this work, the influence of α and n on the path loss in the fruit orchard is studied. Analogous to the sugarcane field case in [10], n, which represents the physical number of the trees (obstructions) along the LOS, is expected as the cause of the angular path loss variation. However, n, unlike n_{r} in Eq. (5), can be counted as 1 only when the LOS of the Tx and Rx is passing through the center of a tree. Therefore, the concept of the equivalent number of trees along the LOS, n_{t}, is introduced to represent n in any angular direction. In other words, the obstruction loss of tree depends on which part of tree that the LOS passes through and n_{t} takes into account this effect. By introducing n_{t}, the X result of each measurement point in Eq. (8) is represented by d, α, and n_{t} as

$$X[d, \alpha, n_{\mathrm{t}}] = L[d, \alpha, n_{\mathrm{t}}] - F(d). \text{ dB} \tag{9}$$

The equivalent vegetation obstruction (EVO) model as the function of n_{t}, instead of d and α, is then proposed to represent the angular excess loss variation as

$$\tilde{X}_{\mathrm{evo}}(n_{\mathrm{t}}) = A_{\mathrm{evo}} \left\{ 1 - \exp\left(-\frac{R_{\mathrm{evo}}}{A_{\mathrm{evo}}} n_{\mathrm{t}} \right) \right\}, \text{ dB} \tag{10}$$

where R_{evo} and A_{evo} are the initial gradient of the attenuation rate of X over n_{t} and the maximum of X, respectively.

5.2. Relative Angular Vegetation Loss of a Single Tree

n_{t} can be determined by using the relative vegetation loss of a single tree, $X_{\mathrm{ts}}[\psi]$, which is the normalized angular excess result of a single tree as

$$X_{\mathrm{ts}}[\psi] = \frac{X[\psi]}{X[\psi = \psi_{\mathrm{ct}}]}, \tag{11}$$

where the angle ψ is the representation of α for a single tree case, and ψ_{ct} is an angle passing through the center line of the tree, e.g., $\psi_{\mathrm{ct}} = 45°$ in Fig. 2. $X_{\mathrm{ts}}[\psi]$ represents n_{t} in each angle of each l^{th} single tree along the LOS, i.e., $n_{\mathrm{t}l}$. Then, the total n_{t} along the LOS in any angular direction can be determined as $n_{\mathrm{t}} = \sum_l n_{\mathrm{t}l}$. More detail of the n_{t} estimation is given in Appendix A.

$X_{\mathrm{ts}}[\psi]$ can be obtained through either the measurement of a single tree as illustrated in Fig. 2 or the Monte Carlo simulation of a single tree using the hybrid T-matrix method that will be described in Subsection 5.3.

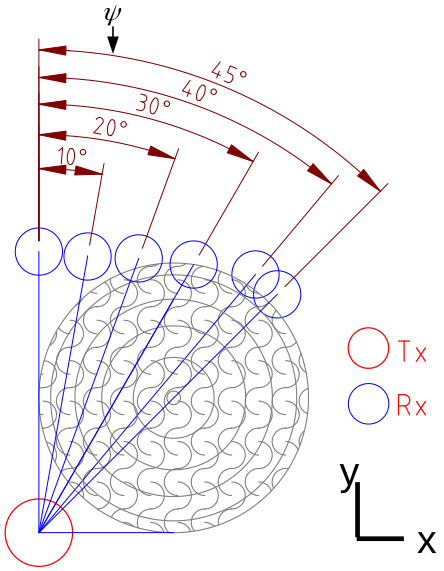

Figure 2. Measurement of a single tree.

5.3. Monte Carlo Simulation Using Hybrid *T*-Matrix

This section describes how to predict $X_{\mathrm{ts}}[\psi]$ by the Monte Carlo simulation of a single jackfruit tree using the hybrid T-matrix method. In the step of determining the T-matrix of each common element in this work, the scattered field of a single scatterer is numerically computed by using SCUFF-EM, a free, open-source software implementation of MOM [29, 30].

5.3.1. Jackfruit Model

A tree model of the jackfruit tree is needed in evaluating the scattered field using hybrid T-matrix. In this investigation, a typical cone trunk and branches of the jackfruit tree are segmented and represented by the cylinder elements as shown in Fig. 3 which is generated by Gmsh, a free, open-source 3D mesh generator [31]. This segmentation is to avoid the irregular meshing of the cone shape in the step of evaluating the scattered field by SCUFF-EM. The leaf is modeled by the dielectric circular disk as shown in Fig. 4.

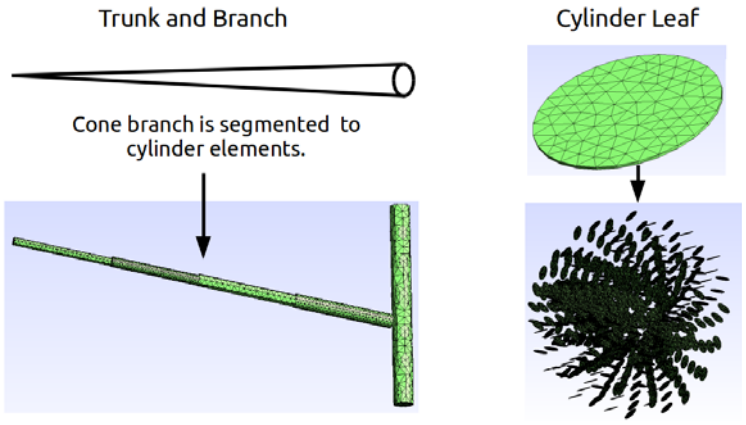

Figure 3. Elements of tree model.

A single tree model is configured on the basis of the following parameters: the main trunk diameter at the level of the Tx and Rx LOS, the circular leaf radius and thickness, and the density. The density is configured as the percentage of the leaves and the branches distributed in three areas of the canopy radius: the outer, middle, and inner. One of the realizations of the jackfruit model is shown in Fig. 4.

5.3.2. Monte Carlo Realization of Jack-Fruit Model

Because the result, which will be presented in Subsection 6.1, reveals that the locations of sub-main branches illustrated in Fig. 5 significantly impact the result of $X_{\mathrm{ts}}[\psi]$, the randomness of these location parameters are emphasized in the Monte Carlo simulation. The tree is vertically segmented into subgroups sub_i as shown in Fig. 5(a). Each sub_i has n_{b} sub-main branches. Fig. 5(b) shows the top view of one realization of the sub-main branch locations in the same subgroup when $n_{\mathrm{b}} = 4$. The location parameters of sub-main branches in terms of azimuth angle, ϕ_{sub}, elevation angle, θ_{sub}, and vertical height, h_{sub}, are illustrated in Figs. 5(b) and 5(c). Note that ϕ_{sub} and θ_{sub} angles are defined on the basis of the spherical coordinate system. Finally, such parameters are randomly generated as follows:

(i) In each sub_i, ϕ_{sub} and h_{sub} are generated according to the uniform distribution. Such values have no any correlation among sub_i.

(ii) Considering the nature of the general trees with a single main trunk, θ_{sub} of the sub-main branches in sub_{i+1} are typically smaller than the values in sub_i. There also exists the overlap angle of θ_{sub} between sub_i and sub_{i+1}. Therefore, the range of θ_{sub} in each sub_i should be specified on the basis of such nature. Then, θ_{sub} values in each sub_i are generated according to the uniform distribution on the basis of its range.

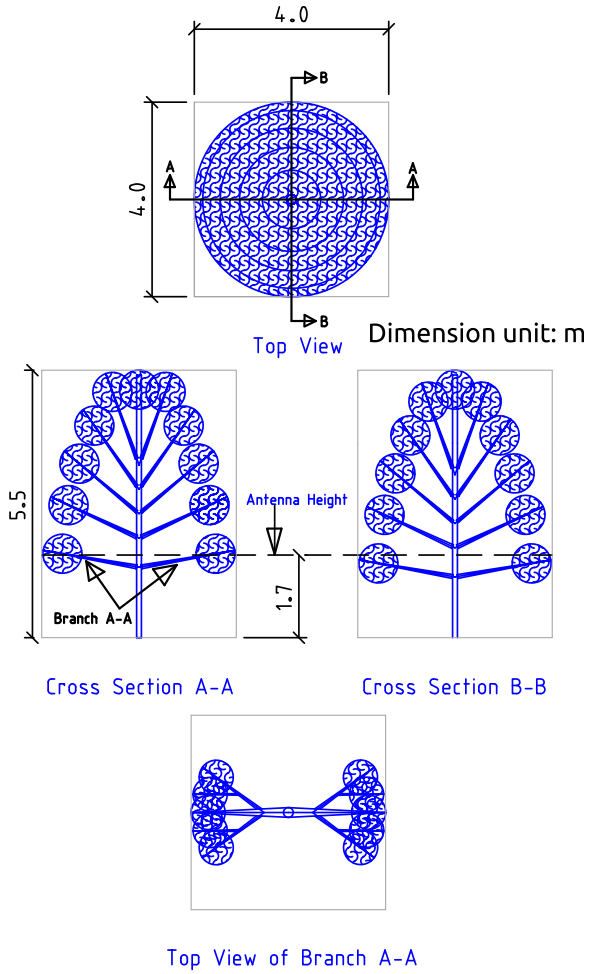

Figure 4. Jackfruit tree model.

5.3.3. Computation of the Relative Angular Vegetation Loss of a Single Tree Using Hybrid T-Matrix

In each realization of the tree model, the total electromagnetic scattered field, due to the incident plane wave illuminating, is computed using the hybrid T-matrix at each observation point. In this work, the simulation scenario illustrated in Fig. 2 is emphasized where the direction of incident plane wave is varied in the azimuth angle step from ψ_1 to ψ_{ct}. Thus, the incident plane wave with propagation direction ψ is defined in time dependence of $\exp(-i\omega t)$ as

$$\vec{E}(\vec{r}) = \vec{E}_0 \exp(i\vec{k} \cdot \vec{r}), \tag{12}$$

where the propagation vector $\vec{k} = k\cos(\frac{\pi}{2} - \psi)\hat{x} + k\sin(\frac{\pi}{2} - \psi)\hat{y}$, the propagation constant $k = \frac{2\pi}{\lambda}$, λ is the wavelength, and $\vec{E}_0$ represents the polarization. The total electromagnetic scattered field at each observation point is the superposition of the scattered field of each element which is determined using the T-matrix method as described in Subsection 2.2. In each direction ψ of the incident plane wave, the total scattered electric field in the forward scattering direction $\vec{E}_{\text{sca}}(\vec{r'})$ is determined, where $\vec{r'} = r'\cos(\frac{\pi}{2} - \psi)\hat{x} + r'\sin(\frac{\pi}{2} - \psi)\hat{y}$, and r' is the observation distance. The angular vegetation loss, X^{sim}, is defined as

$$X^{\text{sim}}(\psi) = \frac{|\vec{E}_{\text{inc}}(\vec{r'})|^2}{|\vec{E}_{\text{inc}}(\vec{r'}) + \vec{E}_{\text{sca}}(\vec{r'})|^2}, \tag{13}$$

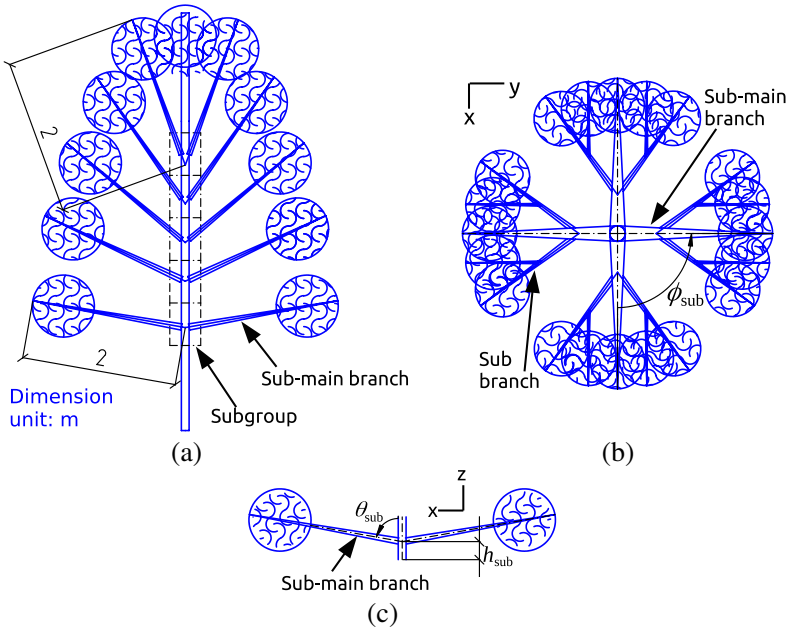

Figure 5. (a) Subgroup segmentation of the main trunk shown as the cross section B-B in Fig. 4. (b) Example of the top view of 4 sub-main branches in a subgroup. (c) One of the subgroups shown as the front view of Fig. 5(a).

where $\vec{E}_{\text{inc}}(\vec{r'}) + \vec{E}_{\text{sca}}(\vec{r'})$ is the total field in the presence of the trees, and the incident field $\vec{E}_{\text{inc}}(\vec{r'})$ represents the total field produced by the sources in the absence of any scatterer [32]. Finally, the relative angular vegetation loss in the case of the simulation, $X_{\text{ts}}^{\text{sim}}[\psi]$, is obtained using Eq. (11).

6. MEASUREMENT AND SIMULATION RESULTS

6.1. Relative Angular Vegetation Loss of a Single Tree Result

$X_{\text{ts}}[\psi]$ results, which are obtained from one case of a single tree measurement, i.e., $X_{\text{ts}}^{\text{mea}}[\psi]$, and from Monte Carlo simulation of a single tree, i.e., $X_{\text{ts}}^{\text{sim}}[\psi]$, are presented in this section. $X_{\text{ts}}^{\text{mea}}[\psi]$ values are determined from results of the measurement points located around the closest tree from the Tx in Fig. 1(b) with $\psi = \{0°, 10°, 20°, 30°, 40°, 45°\}$.

In the Monte Carlo simulation, the single tree model is configured the same as the jackfruit tree presented in the measurement as much as possible. The relative permittivity, ϵ_{r}, of the tree's elements is configured at 10 which is the same as the value used in [14, 15]. However, this constant is not seriously considered in this work because the relative value of the scattered field, not the absolute value, is investigated. The total height of the main trunk and its diameter at the level of the Tx and Rx LOS are 5.5 m and 0.1 m, respectively. The length of each sub-main branch is 2 m as illustrated in Fig. 5(a). In each group of the sub-main branch, there are two levels of the sub branch length: 1 m and 0.5 m as illustrated in Fig. 5(b). The orientation of each sub-main branch is generated randomly as described in Subsection 5.3.2, but orientations of its sub branches are fixed. The circular leaf radius and thickness are 3 cm and 1 mm, respectively. The leaf orientation is generated randomly on the basis of the uniform distribution. The leaves and small branches are densely distributed at approximately 30% of the outer radius area of the canopy. In addition, the densities of the leaves and branches are sparse in the middle of the radius, and the big trunk is located at the center of the canopy. sub_1 is started at 1.1 m above the ground, and each sub_i occupies 0.55 m of the vertical interval of the trunk. There are totally 5 subgroups. Each sub_i has $n_{\text{b}} = 4$. The specific range for θ_{sub} in each sub_i is defined as $\{\text{sub}_1, \text{sub}_2, \text{sub}_3, \text{sub}_4, \text{sub}_5\} = \{90° \leq \theta_{\text{sub}} \geq 70°, 75° \leq \theta_{\text{sub}} \geq 55°, 60° \leq \theta_{\text{sub}} \geq 40°, 45° \leq \theta_{\text{sub}} \geq 25°, 30° \leq \theta_{\text{sub}} \geq 10°\}$ where the overlap angle between sub_i and sub_{i+1} is 5°. The direction of incident

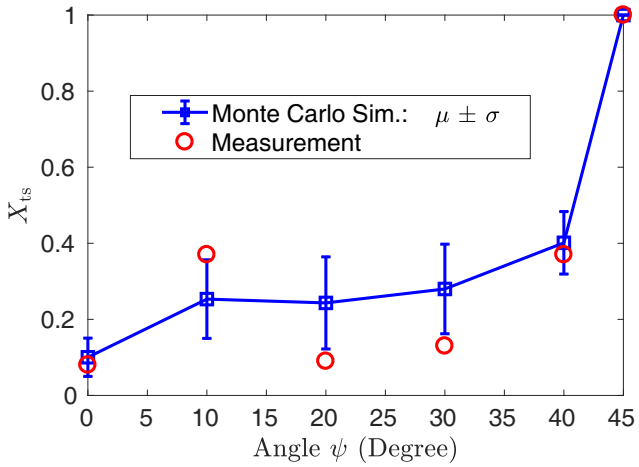

Figure 6. Comparison of $X_{ts}[\psi]$ results obtained from the measurement and the Monte Carlo simulation.

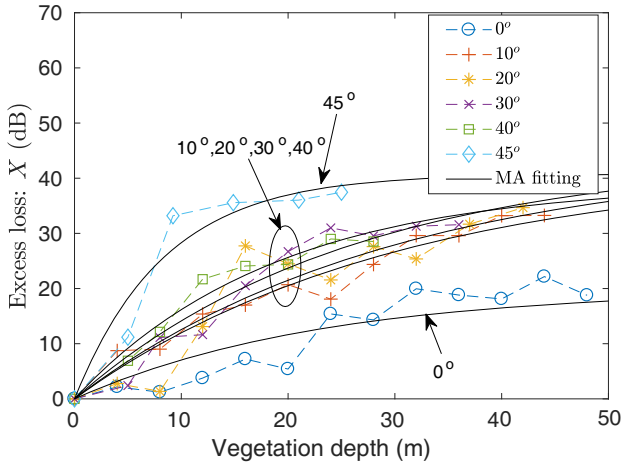

Figure 7. Excess loss values fitted with MA model.

plane wave is varied in the azimuth angle step the same as the measurement. Using Eqs. (13) and (11), $X_{ts}^{sim}[\psi]$ are computed from 20 realizations of the tree model.

The comparison between $X_{ts}^{mea}[\psi]$ and $X_{ts}^{sim}[\psi]$ results is presented in Fig. 6. The closest results between them are found to be the realization of Fig. 4 where the significant loss is also observed in 10° direction. Considering the cross section A-A in Fig. 4, the high loss in this angular direction is because the dense area of the leaves and small branches in the outer radius of the sub-main branch A-A directly obstruct the Tx-Rx LOS in the measurement, i.e., the forward scattering direction in the simulation, whereas there is no big obstruction in 20° and 30° directions. This points out that the locations of the sub-main branches significantly impact on the result of $X_{ts}[\psi]$. This also suggests that the $X_{ts}[\psi]$ result obtained from only one case of a single tree measurement might not be able to represent the general effect due to the branch locations. On the other hand, the average of $X_{ts}^{sim}[\psi]$ of all the 20 tree realizations in 10° direction becomes smaller than the realization of Fig. 4, while the losses in 20° and 30° become higher.

6.2. Path Loss Result

The results of the excess loss X obtained using Eq. (9) are firstly represented by MA model (3), one of the existing empirical model, as shown in Fig. 7. It is obvious that a different MA model is needed to represent X values in each angular direction due to the high variation over α, whereas the X values in all angular directions can be represented by one equation of the proposed EVO model of Eq. (10) as shown in Fig. 8. The fitting results of X using EVO model as a function of n_t^{mea} and n_t^{sim} are shown in Figs. 8(a) and 8(b), respectively. These n_t^{mea} and n_t^{sim} are n_t obtained on the basis of $X_{ts}^{mea}(\psi)$ and $X_{ts}^{sim}[\psi]$ results as described in Subsection 5.2 and Appendix A, respectively. Obviously, n_t is the cause of the angular path loss variation. In the case of fitting X values of all α directions over n_t^{mea}, the EVO is expressed as

$$\tilde{X}_{evo}(n_t^{mea}) = 38.8\left\{1 - \exp\left(-\frac{28.3}{38.8}n_t^{mea}\right)\right\} + N(0, 3.9),\ \text{dB} \tag{14}$$

where $N(\mu, \sigma)$ represents the normally distributed random variable with mean μ and standard deviation σ. In the case of fitting X values of all α directions over n_t^{sim}, the EVO is expressed as

$$\tilde{X}_{evo}(n_t^{sim}) = 39.1\left\{1 - \exp\left(-\frac{26.1}{39.1}n_t^{sim}\right)\right\} + N(0, 3.6).\ \text{dB} \tag{15}$$

As the explanation of the VO model in [10], this EVO model also exhibits two gradients of attenuation rate: a greater rate at small n_t and a smaller rate at larger n_t. Because n_t represents the magnitude of

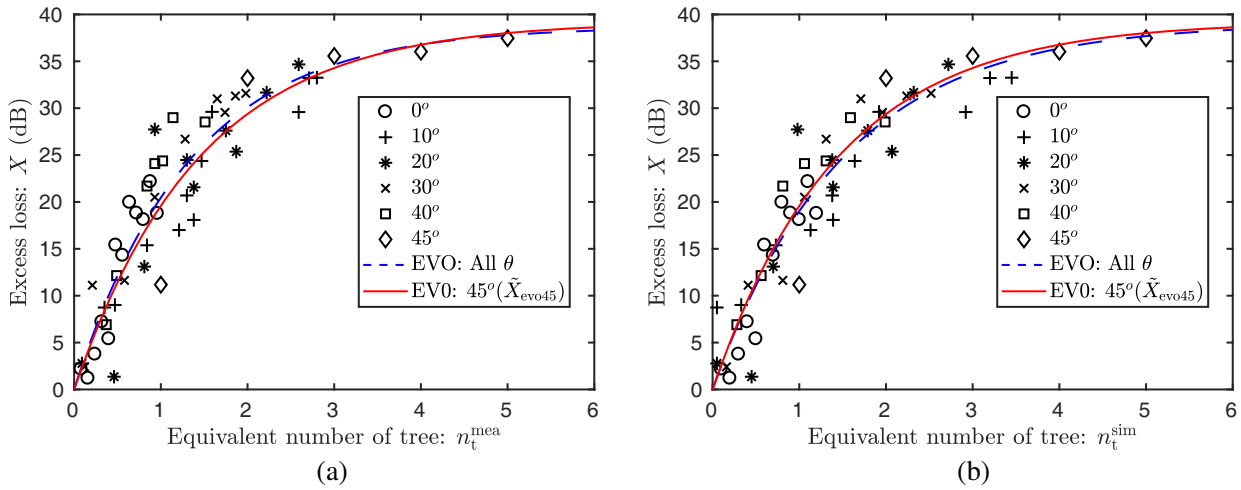

Figure 8. The plot of X over (a) $n_t = n_t^{mea}$ and (b) $n_t = n_t^{sim}$.

vegetation length, which is analogous to the vegetation depth d, the EVO model in Eq. (10) can also be described by the interplay of the coherent and incoherent components of radio propagation in the vegetation medium regarding RET model as explained in [10, Subsection 2.1.1].

The EVO fitting on X values of an only $\alpha = 45°$ data set, i.e., $\tilde{X}_{evo45}$, is also shown as the reference in Fig. 8. In this direction, n_t exactly represents the physical number of trees, i.e., n, because the LOS passes through the center of all trees. Then, n_t^{mea} and n_t^{sim} are the same. Thus, $\tilde{X}_{evo45}$ lines in Figs. 8(a) and 8(b) are also the same. This $\tilde{X}_{evo45}$ is expressed as

$$\tilde{X}_{evo45}(n_t) = 39.2\left\{1 - \exp\left(-\frac{27.1}{39.2}n_t\right)\right\} + N(0, 3.6).\ \text{dB} \tag{16}$$

The error term, $N(\mu, \sigma)$, in Eq. (16) is the difference between the $\tilde{X}_{evo45}$ line and the data set of X result in $\alpha = 45°$, whereas the statistic values of the error between the $\tilde{X}_{evo45}$ line and the data set of X result in all angular directions are shown as follows:

- $n_t = n_t^{mea}$: $N(\mu, \sigma) = N(0.2, 4.0)$, RMSE $= 4.0$ dB.
- $n_t = n_t^{sim}$: $N(\mu, \sigma) = N(-0.2, 3.7)$, RMSE $= 3.7$ dB.

It is obvious that $\tilde{X}_{evo45}$ can be used to predict the X values in other angular directions. The means of the error values in the two cases show the same distance from zero value but in different directions, while the standard deviation and root-mean-square error (RMSE) of the error values for the n_t^{sim} case are smaller. On the basis of this error evaluation, as well as the results presented in Subsection 6.1 which pointed out that using $X_{ts}[\psi]$ result from only one case of a single tree measurement might not be able to represent the general effect due to the randomness of branch locations, and both suggest that the Monte Carlo simulation for the randomness of a single tree by using hybrid T-matrix is an alternative approach to obtain $X_{ts}[\psi]$ in order to reduce the measurement effort.

7. PATH LOSS PREDICTION AT ANY POINT IN THE FRUIT ORCHARD

By utilizing the EVO model proposed and explained previously, the procedure of predicting the path loss at any point in the fruit orchard by making a few measurement efforts can be formulated. This approach practically makes the WSN planning and management easier. The procedure can be described as follows:

(i) The first step is to obtain the results of the excess loss X in an only 45° direction, by either the dedicated measurement or the derivation of the values on the basis of the received signal strength indication (RSSI) collected from the existing wireless sensor nodes in the orchard.

(ii) Second, the EVO model in 45°, $\tilde{X}_{\text{evo45}}(n_{\text{t}})$, is estimated by fitting the X results obtained in the first step over n_{t}, where $n_{\text{t}} = n$ in this angular direction. Based on the measurement result described previously, this estimated $\tilde{X}_{\text{evo45}}(n_{\text{t}})$ can be applied to every angle.

(iii) Third, the measurement or Monte Carlo simulation using hybrid T-matrix of a single tree is necessary in order to determine X_{ts}. Using the planting pattern of considering fruit orchard and applying the approach described in Subsection 5.2 and Appendix A on the obtained X_{ts}, the values of d and n_{t} along the LOS of any Tx-Rx locations are obtained.

(iv) Finally, using the d and n_{t} values obtained in the third step, the path loss at any points in the fruit orchard can be predicted by the model expressed as

$$\tilde{L}(d, n_{\text{t}}) = F(d) + \tilde{X}_{\text{evo45}}(n_{\text{t}}),\ \text{dB} \tag{17}$$

where $\tilde{X}_{\text{evo45}}(n_{\text{t}})$ is the EVO model obtained in the second step.

This prediction procedure can be applied adaptively in any fruit orchards at any d_{s} under the specific conditions as follows:

(i) The trees have the same age of growth. Therefore, the leaf, canopy, and trunk size are not significantly different over the trees.

(ii) The trees are planted in a grid pattern. This characteristic is obvious in most of the cases of fruit orchard, but it is not true in the forest environment. Although this approach is unable to apply directly to the planting patterns other than the grid, the proposed approach might be applied in other patterns, which are not planted randomly, with some modifications of d_{s} parameter described in Appendix A.

(iii) The trees must be higher than antenna height. This approach is not applicable to the initial growth stage of the fruit orchard where the antenna height might be higher than the trees.

Although further experimental validation is needed, the same procedure is expected to be applicable to other fruit orchards under the above conditions.

8. CONCLUSION

This paper presented the analysis of path loss result and proposed the path loss prediction in the jackfruit orchard representing the fruit orchard which is one of the common types of agriculture environment. The path loss measurement was conducted at 2.45 GHz band. The location of Tx in the measurement was fixed, and then the Rx was moved over the vegetation depth, d, and angular direction, α. This measurement scenario allowed investigating the excess loss X, i.e., path loss value that exceeds the free space loss, over the angular direction, α, and the number of trees along the LOS of the Tx and Rx, n. The significant conclusions of this work are summarized as follows:

- Due to the angular dependence of n of the fruit trees, this work introduced the equivalent number of trees, n_{t}, to represent the magnitude of vegetation obstruction along the LOS in any α.
- This work proposed the approach to estimate n_{t} using the relative vegetation loss of a single tree, X_{ts}.
- The high variation of X values over α directions, i.e., angular dependence excess loss, was observed.
- n_{t} was found to be the reason for the angular dependence excess loss because there exists the same relationship between X and n_{t} in every α.
- The equivalent vegetation obstruction (EVO) model as a function of one parameter (n_{t}), instead of two parameters (d and α), is proposed to better represent the angular variation of X.
- The prediction procedure of the path loss at any point in the orchard that employs a few measurement efforts was proposed on the basis of the EVO model.
- Although X_{ts} result, which is used to determine n_{t}, can be obtained from the measurement of a single tree, this work introduced the Monte Carlo simulation of a single tree using hybrid T-matrix. The evaluation in terms of prediction error pointed out that the Monte Carlo simulation is the alternative approach to further reduce the measurement efforts required for the proposed path loss prediction approach.

ACKNOWLEDGMENT

This work was partly supported by the Fujikura Foundation. The authors would like to thank Miss. Boonpluk Pongsiri, the owner of the jackfruit orchard, for allowing and supporting the measurements.

APPENDIX A. EQUIVALENT NUMBER OF TREE

Using $X_{\mathrm{ts}}[\psi]$, the n_{t} can be determined as follows:

- The angular areas, Ar, are separated and illustrated as Fig. A1, where the outer radius of such area is defined by Eq. (A1). By utilizing Ar, if the LOS along Tx and Rx passes through the Ar $= 10^{\circ}$ area of the l^{th} tree, it means that $n_{tl} = X_{\mathrm{ts}}[\psi = 10^{\circ}]$.
- For $\psi = \psi_1, \psi_2, \ldots, \psi_Q$, $\psi_q > \psi_{q-1}$ and $\psi_Q = \psi_{\mathrm{ct}}$, r_ψ is defined as the outer radius for Ar of ψ and expressed as

$$r_{\psi=\psi_q} = \begin{cases} \dfrac{d_{\mathrm{s}}}{2} & \psi_q = 0 \\ \dfrac{d_{\mathrm{s}}}{2} - \dfrac{d_{\mathrm{s}}}{2}\tan\left(\psi_q - \dfrac{\psi_q - \psi_{q-1}}{2}\right) & \psi_q > 0, q > 1, \end{cases} \tag{A1}$$

  where d_{s} is the distance between the centers of two trees as illustrated in Fig. A2.

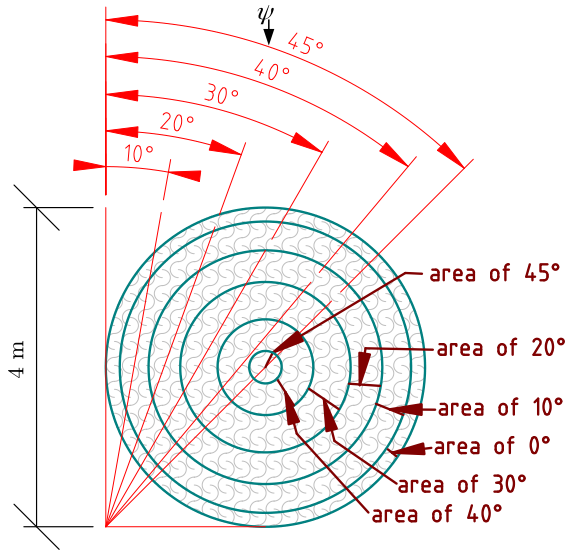

Figure A1. Definition of angular area for a single tree.

Considering Fig. A2, let define the grid point as the intersection point of the tangent lines that connect two adjacent circles with diameter d_{s}. The center of each circle is at the center point of the tree. The origin point of the x-y coordinate is defined as the grid point which is closest to the Tx location. Then, the Tx and Rx locations are defined as (x_{tx}, y_{tx}) and (x_{rx}, y_{rx}), respectively. This Tx is located at either the origin point or non-origin point, but it typically does not coincide with the canopy area as illustrated in Figs. A2(a) and A2(b), respectively. The LOS along the Tx and Rx can be expressed in the typical linear equation as $ax + by + c = 0$, where $a = \tan(\frac{\pi}{2} - \alpha)$, $b = -1$, $c = y_{\mathrm{tx}} - x_{\mathrm{tx}}a$ and $\alpha = \tan^{-1}(\frac{y_{\mathrm{rx}} - y_{\mathrm{tx}}}{x_{\mathrm{rx}} - x_{\mathrm{tx}}})$. Then, one can find the closest distance, r_{c}, which is illustrated in Fig. A2, from the center point (x_l, y_l) of the considering l^{th} tree to such LOS line as

$$r_{\mathrm{c}l} = \frac{|ax_l + by_l + c|}{\sqrt{a^2 + b^2}}. \tag{A2}$$

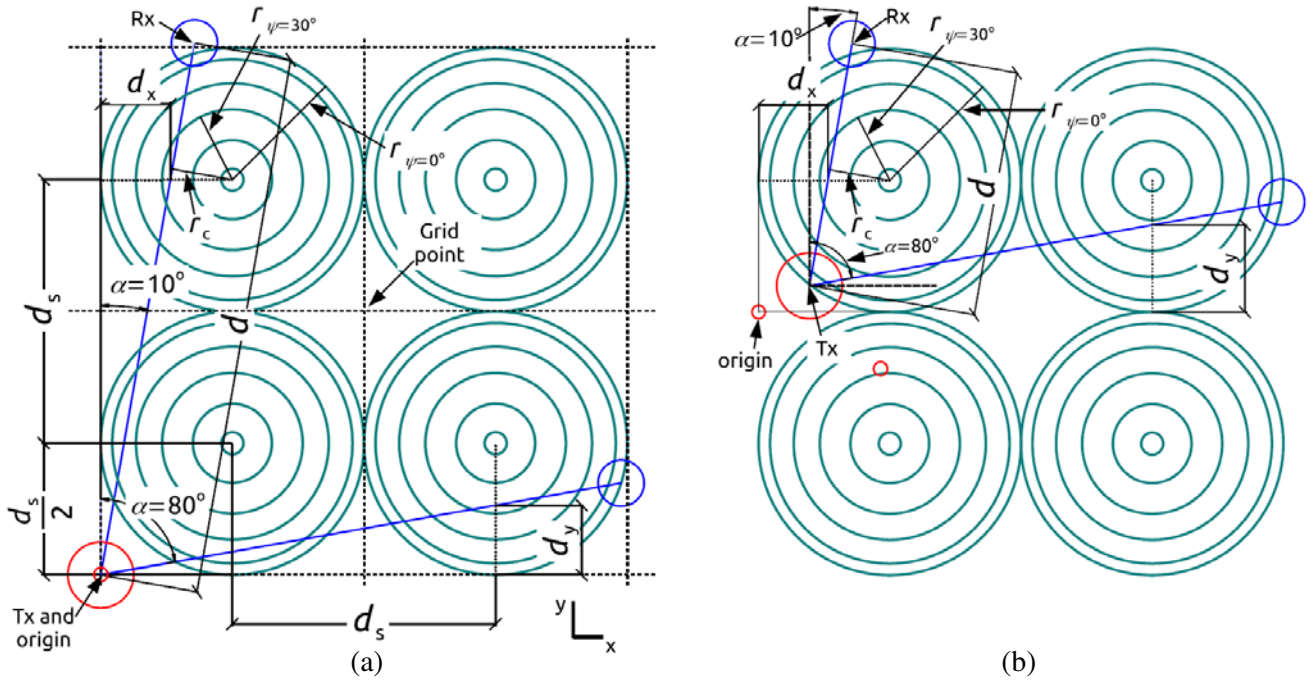

Figure A2. Dimension terms for the algorithm of determining Ar and n_t. (a) Tx located at origin point (b) Tx located at non-origin point.

Thus, by searching through each l^{th} tree in LOS direction and comparing its r_{cl} with the r_ψ in Eq. (A1), one can find Ar_l whose LOS passes through as

$$\text{Ar}_l = \max(\psi) \text{ such that } r_\psi \geq r_{cl} \tag{A3}$$

Finally, $n_t = \sum_l n_{tl}$, where $n_{tl} = X_{ts}[\text{Ar}_l]$.

REFERENCES

1. Bongiovanni, R. and J. Lowenberg-Deboer, "Precision agriculture and sustainability," *Precision Agriculture*, Vol. 5, No. 4, 359–387, Aug. 2004.
2. Ndzi, D. L., A. Harun, F. M. Ramli, M. L. Kamarudin, A. Zakaria, A. Y. M. Shakaff, M. N. Jaafar, S. Zhou, and R. S. Farook, "Wireless sensor network coverage measurement and planning in mixed crop farming," *Computers and Electronics in Agriculture*, Vol. 105, 83–94, 2014.
3. Savage, N., D. Ndzi, A. Seville, E. Vilar, and J. Austin, "Radio wave propagation through vegetation: Factors influencing signal attenuation," *Radio Science*, Vol. 38, No. 5, n/a–n/a, Oct. 2003.
4. Joshi, G. G., C. B. Dietrich, C. R. Anderson, W. G. Newhall, W. A. Davis, J. Isaacs, and G. Barnett, "Near-ground channel measurements over line-of-sight and forested paths," *IEE Proceedings — Microwaves, Antennas and Propagation*, Vol. 152, No. 6, 589–596, Dec. 2005.
5. Gay-Fernández, J. A., M. Garcia Sánchez, I. Cuinas, A. V. Alejos, J. G. Sanchez, and J. L. Miranda-Sierra, "Propagation analysis and deployment of a wireless sensor network in a forest," *Progress In Electromagnetics Research*, Vol. 106, 121–145, 2010.
6. Gay-Fernández, J. A. and I. Cuiñas, "Peer to peer wireless propagation measurements and path-loss modeling in vegetated environments," *IEEE Transactions on Antennas and Propagation*, Vol. 61, No. 6, 3302–3311, Jun. 2013.
7. Oestges, C., B. M. Villacieros, and D. Vanhoenacker-Janvier, "Radio channel characterization for moderate antenna heights in forest areas," *IEEE Transactions on Vehicular Technology*, Vol. 58, No. 8, 4031–4035, Oct. 2009.

8. Gay-Fernández, J. A. and I. Cuiñas, "Short-term modeling in vegetation media at wireless network frequency bands," *IEEE Transactions on Antennas and Propagation*, Vol. 62, No. 6, 3330–3337, Jun. 2014.
9. ITU-R P.833-9, "Attenuation in vegetation," Sep. 2016.
10. Srisooksai, T., K. Kaemarungsi, J. Takada, and K. Saito, "Radio propagation measurement and characterization in outdoor tall food grass agriculture field for wireless sensor network at 2.4 GHz band," *Progress In Electromagnetics Research C*, Vol. 88, 43–58, 2018.
11. Ndzi, D. L., L. M. Kamarudin, A. A. Muhammad Ezanuddin, A. Zakaria, R. B. Ahmad, M. F. B. A. Malek, A. Y. M. Shakaff, and M. Jafaar, "Vegetation attenuation measurements and modeling in plantations for wireless sensor network planning," *Progress In Electromagnetics Research B*, Vol. 36, 283–301, 2012.
12. Balachander, D., T. R. Rao, and G. Mahesh, "RF propagation experiments in agricultural fields and gardens for wireless sensor communications," *Progress In Electromagnetics Research C*, Vol. 39, 103–118, 2013.
13. Hara, M., H. Shimasaki, Y. Kado, and M. Ichida, "Effect of Vegetation growth on radio wave propagation in 920-MHz band," *IEICE Transactions on Communications*, Vol. 99, No. 1, 81–86, 2016.
14. Co, P. J. and J. Takada, "Hybrid T-matrix modeling of electromagnetic scattering from simplified leaf structures," *2016 Progress In Electromagnetic Research Symposium (PIERS)*, 3210–3210, Shanghai, China, Aug. 8–11, 2016.
15. Co, P. J., "Spherical wave expansion approach to modeling the radio wave propagation effects of foliage," Ph.D. dissertation, Tokyo Institute of Technology, Japan, Mar. 2018.
16. IEEE Std 802.15.4-2015 (Revision of IEEE Std 802.15.4-2011), IEEE Standard for Low-Rate Wireless Networks, IEEE2006, Apr. 2016.
17. Meng, Y. S. and Y. H. Lee, "Investigations of foliage effect on modern wireless communication systems: A review," *Progress In Electromagnetics Research*, Vol. 105, 313–332, 2010.
18. COST 235 Management Committee, COST 235 Radiowave Propagation Effects on Nextgeneration Fixed-Services Terrestrial Telecommunications Systems, 1996.
19. Seville, A. and K. H. Craig, "Semi-empirical model for millimetre-wave vegetation attenuation rates," *Electronics Letters*, Vol. 31, No. 17, 1507–1508, Aug. 1995.
20. Yee, K., "Numerical solution of initial boundary value problems involving Maxwell's equations in isotropic media," *IEEE Transactions on Antennas and Propagation*, Vol. 14, No. 3, 302–307, May 1966.
21. Harrington, R. F., "Field computation by moment methods," *ser. IEEE Press series on Electromagnetic Waves, IEEE, Inc. [u.a.]*, New York, NY, 2000, oCLC: 255758693.
22. Johnson, R. and F. Schwering, "A transport theory of millimeter wave propagation in woods and forests," *US Army, Comumunications-Electronics Command*, Fort Monmouth, New Jersey, Tech. Rep. CECOM-TR-85-1, 1985.
23. Fernandes, T. R., R. F. Caldeirinha, M. Al-Nuaimi, and J. Richter, "A discrete RET model for millimeter-wave propagation in isolated tree formations," *IEICE Transactions on Communications*, Vol. E88-B, No. 6, 2411–2418, Jun. 2005.
24. Waterman, P. C., "Matrix formulation of electromagnetic scattering," *Proceedings of the IEEE*, Vol. 53, No. 8, 805–812, Aug. 1965.
25. "Electromagnetic simulation software, Altair FEKO," https://altairhyperworks.com, accessed May 25, 2018.
26. Naganawa, J., K. Haneda, M. Kim, T. Aoyagi, and J. Takada, "Antenna deembedding in FDTD-based radio propagation prediction by using spherical wave function," *IEEE Transactions on Antennas and Propagation*, Vol. 63, No. 6, 2545–2557, Jun. 2015.
27. Srisooksai, T., J. Takada, and K. Saito, "Portable wide-band channel sounder based software defined radio for studying the radio propagation in an outdoor environment," *2017 International Symposium on Antennas and Propagation (ISAP)*, 1–2, Oct. 2017.

28. Kaemarungsi, K., "Development and deployment of ZigBee wireless sensor networks for precision agriculture in sugarcane field," *33rd Asia-Pacific Advanced Network (APAN)*, Feb. 2012.
29. Homer Reid, M. T. and S. G. Johnson, "Efficient computation of power, force, and torque in BEM scattering calculations," ArXiv e-prints, Jul. 2013.
30. "SCUFF-EM website," accessed May 29, 2018, http://github.com/homerreid/scuff-EM.
31. Geuzaine, C. and J.-F. Remacle, "Gmsh: A 3-D finite element mesh generator with built-in pre- and post-processing facilities," *International Journal for Numerical Methods in Engineering*, Vol. 79, No. 11, 1309–1331, Sep. 2009.
32. Balanis, C. A., *Advanced Engineering Electromagnetics*, 2nd edition, Wiley, Hoboken, NJ, 2012.